

Regional Clock Tree Generation by Abutment in Synchoros VLSI Design

Dimitrios Stathis^{a,*}, Panagiotis Chaourani^a, Syed M. A. H. Jafri^a, Ahmed Hemani^a
^aKTH Royal Institute of Technology, Electrum 229, 164 40 Kista, Stockholm, Sweden
 Email: stathis, pancha, jafri, hemani@kth.se

Abstract—Synchoros VLSI design style has been proposed as an alternative to standard cell-based design. Standard cells are replaced by synchoros large grain VLSI design objects called SiLago blocks. This new design style enables end-to-end automation of large scale designs by abutting the SiLago blocks to eliminate logic and physical synthesis for the end-users. A key problem in this automation process is the generation of regional clock tree. Synchoros design style requires that the clock tree should emerge by abutting its fragments. The clock tree fragments are absorbed in the SiLago blocks as a one-time engineering effort. The clock tree should not be ad-hoc, but a structured and predictable design whose cost metrics are known. Here, we present a new clock tree design that is compatible with the synchoros design style. The proposed design has been verified with static timing analysis and compared against functionally equivalent clock tree synthesised by the commercial EDA tools. The scheme is scalable and, in principle, can generate arbitrarily complex designs. In this paper, we show as a proof of concept that a regional clock tree can be created by abutment. We prove that with the help of the generated clock tree, it is possible to generate valid VLSI designs from 0.5 to ~2 million gates. The resulting generated designs do not need a separate regional clock tree synthesis. More critically, the synthesised design is correct by construction and requires no further verification. In contrast, the state-of-the-art hierarchical synthesis flow requires synthesis of the regional clock tree. Additionally, the conventional clock tree and its design needs a verification step because it lacks predictability. The results also demonstrate that the capacitance, slew and the ability to balance skew of the clock tree created by abutment is comparable to the one generated by commercial EDA tools.

Index Terms— CGRA, Clock Tree Synthesis, Composition by Abutment, EDA, VLSI Design, SiLago, Synchoricity

I. INTRODUCTION

In this paper, we present a clock tree generation scheme for a novel *synchoros* VLSI (Very Large Scale Integration) design framework. Synchoros VLSI design is an alternative to the standard cell-based VLSI design framework. The word synchoros is derived from the Greek word for space – *χώρα* (khôros). Synchoricity is analogous to synchronicity. In synchronous systems, time is discretised with clock ticks to enable temporal composition of synchronous datapaths. In synchoros systems, space is discretised uniformly with a virtual grid. This virtual grid enables the spatial composition of the system by abutting synchoros building blocks, that we call SiLago (Silicon Lego bricks) blocks. All wires, including the clock, are absorbed within the SiLago blocks. When a system is composed by abutting SiLago blocks, a valid DRC (Design

Rule Checking) and timing clean GDSII (Graphic Database System II) is generated. The design does not need any further VLSI engineering, other than what has gone into creating the SiLago blocks as a one-time engineering effort. In essence, SiLago blocks are the new mega standard cells.

The need for synchoros VLSI design style, as a replacement for standard-cell-based VLSI design, is elaborated in section II. Briefly, the key benefits of synchoros VLSI design style are:

1. End-to-end automation of complex system-models to GDSII; complex system models imply 100+ million gate complexity and non-deterministically concurrent untimed applications
2. Computational efficiency similar to application-Specific Integrated Circuit (ASIC) [1]
3. Programming comparable engineering effort with correct-by-construction and near-perfect prediction of cost metrics,
4. Sufficient flexibility for in-field bug fixes and version updates
5. Foundry compatible design
6. Potential to eliminate mask engineering cost and significantly lower silicon and engineering cost related to DFT (Design For Test).

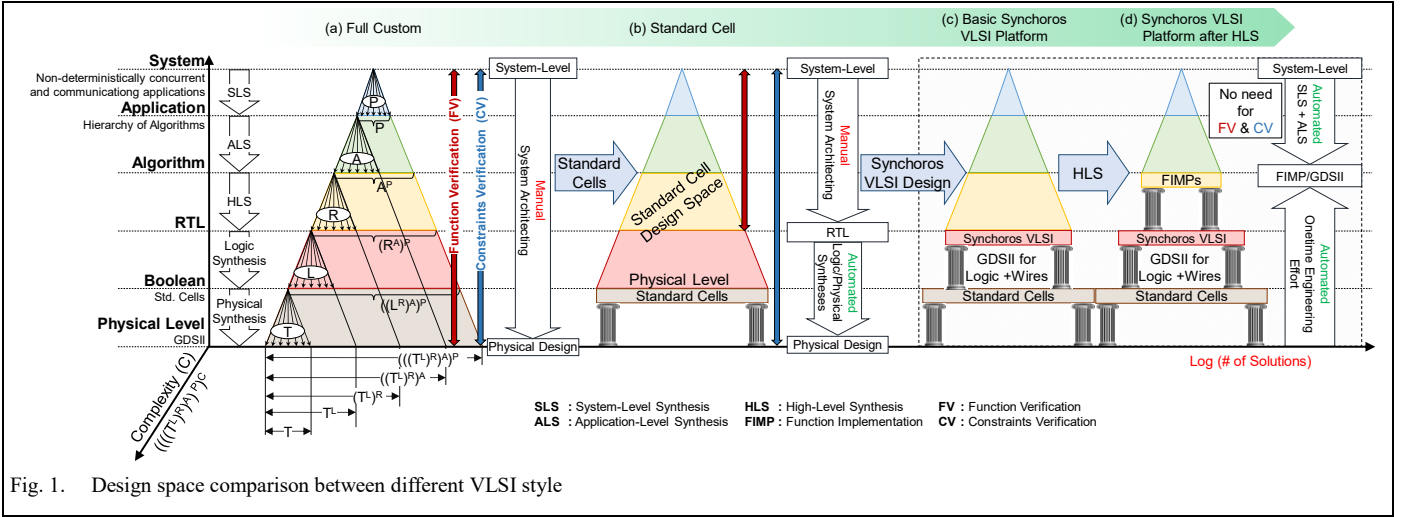
Clocks in synchoros VLSI designs have three levels of hierarchy. In the highest level of hierarchy is the global clock that is derived from PLL and distributed to region instances. The region instances roughly correspond to chiplets or sub-systems in traditional SOC architectures. They communicate with each other on a latency insensitive basis. Each region instance is composed of SiLago blocks that communicate with each other on a synchronous basis fed by a regional clock tree (RCT). RCT is the focus of this paper and constitutes the second level on the hierarchy of clocks. The lowest level of the hierarchy is the clock tree in the SiLago block, which is synthesised by commercial EDA tools.

In this paper, we focus on a critical aspect of synchoros VLSI design style – the generation of valid RCT by abutment of SiLago blocks. The proposed RCT generation-by-abutment scheme does not compete with the existing clock tree synthesis schemes on traditional figure-of-merits. Instead, the proposed scheme obviates the need for RCT synthesis.

The key contributions in this paper are:

- a. We present a design that allows the RCT to be divided into fragments that are absorbed as part of the synchoros SiLago blocks. When these blocks abut, a valid RCT gets created. No additional step, like clock tree synthesis of the traditional standard cells based design flow, is needed.
- b. The generated RCT and the synchoros SiLago based design is correct-by-construction and does not require any further

* Corresponding author



verification by static timing analysis or DRC.

- c. The generated RCT is predictable in terms of its switching capacitance, arrival time, slew and skew at each leaf node, i.e., the SiLago block.
- d. The generated RCT has comparable cost metrics - capacitance, skew and slew- to a functionally equivalent RCT generated by commercial EDA tools.

The roadmap for the rest of the paper is as follows: In the next section II, we justify the need for synchoros VLSI design style as a replacement for standard cell-based VLSI design. In section III, we introduce a synchoros VLSI design platform as the background in which the proposed RCT scheme has been developed. In the same section, we also introduce the demands for RCT generation in a synchoros VLSI design platform. Sections II and III give an overview of the basics of the synchoros VLSI design style and serve as the motivation and basis for this work. In section IV, we elaborate the proposed RCT generation-by-abutment scheme, and in section V, we explain the process of configuring the RCT. In section VI, we quantify the benefits and cost of RCT, compare it to a functionally equivalent clock tree generated by commercial EDA tools and provide proof-of-concept experimental results for the predictability of the generated RCT. In section VII, we review the state-of-the-art in clock tree synthesis and argue why these techniques do not meet the requirements for RCT generation in the synchoros VLSI design style. Finally, we conclude and point to the ongoing enhancements of the SiLago platform.

II. THE NEED FOR SYNCHOROS VLSI DESIGN

Synchoros VLSI design style is needed to make ASIC-like performance and computational efficiency affordable to even small actors. This is made possible by enabling end-to-end automation and eliminating the need for logic and physical synthesis by the end-user. The problem addressed in this paper is a critical sub-problem in enabling synchoros VLSI design style.

ASICs outperform software-based implementations by 2-3 orders [2]. The need for ASIC-like efficiency is acutely felt in all domains of the industry[3 - 8]. The principal reason for not adopting ASICs has been the large cost, of which 90% is engineering [12]. Furthermore, designing ASIC requires

specialist competence, expensive and difficult to use EDA tools and a long lead time. All these factors add up to ASICs being accessible only to large actors like Google, that opted for an ASIC style implementation for its TPU. Even making an accelerator rich and software-centric custom SOC is too expensive for small actors. As a result, small actors are forced to adopt FPGAs and GPUs that seldom deliver the required power-performance [13].

A. Challenges with state-of-the-art EDA flows

We next analyse why standard cell-based EDA flows have not scaled with complexity. This analysis is done in terms of the VLSI design space, shown in Fig. 1. We argue that this design space increases exponentially with complexity and impedes design automation. The key contributions of the synchoros design style are a) to sufficiently reduce this design space and b) to make this reduced design space composable and predictable. These contributions enable end-to-end design automation of complex applications and systems. The final custom design has ASIC comparable performance and efficiency.

The VLSI design space that is shown in Fig. 1 has three dimensions. Abstraction and complexity are the independent variables, and the number of solutions is an exponential function of the two independent variables. There are six levels of abstraction, as shown in Fig. 1. Synthesis is the process of refining from more abstract to more detailed and proceeds in a top-down manner, by successively refining the functionality from one level to the next lower level. At each level, the refinement process evaluates multiple functionally equivalent implementation alternatives. These implementations are expressed in terms of building blocks at the next lower level of abstraction. As this process continues the number of design alternatives increases exponentially at each level, as shown in Fig. 1. By the time physical synthesis happens, the design space has expanded to $((T^L)^R)^A)^P$. Complexity C further increases this space to $((T^L)^R)^A)^P)^C$.

The top-down refinement process implies that the real cost of a design is not known until it has been refined down to the physical level. At higher abstractions, when multiple solutions are evaluated, the evaluations are based on estimated cost-metrics. The accuracy of these estimates degrade with increasing abstraction level and complexity of the functionality.

This exponential increase in design space and the exponential degradation in accuracy of cost-metrics, which are used to explore the design space, together with an increase in abstraction and complexity is the fundamental VLSI design challenge. All progress in VLSI design automation can be cast in terms of attempts to solve the fundamental VLSI design challenge.

In the full-custom era, shown in Fig. 1a, the entire design space from the system down to the physical level was manually refined. Despite Mead Conway’s structured VLSI design style [14] and later attempts to automate the process using silicon compilers. The full custom design space was too large for design automation. This restricted the design to $\mathcal{O}(10K)$ gates.

Standard cells were introduced to reduce the design space and to enable a higher degree of automation. That allowed the complexity of the systems to go beyond what was possible with full-custom design style. The reduction of the design space was achieved by standardising all boolean level logic as a set of one-time engineered set of standard cells. This effectively raised the physical design to boolean level, i.e., as soon as a design is at a boolean level, we know its physical design. However, the wires that connect these standard cells, clock them, reset them etc. are not known. They have to be synthesised as part of physical synthesis. *In synchoros VLSI design style all wires, functional and infrastructural, get created by abutment rather than in a follow-up physical synthesis step.*

Despite imperfectly raising the physical design to boolean level, standard cells succeeded in automating synthesis from RTL down to physical level. The Achilles heel of the standard cell design flow is that the refinement from system-level down to RTL is done manually. For ASICs, this refinement is in terms of functional RTL designs, and for SOCs, this refinement is in terms of infrastructural IPs. This manual refinement requires costly functional verification to ensure that the system model is preserved in the manually refined RTL model. Furthermore, manual refinement is done using crude estimates that can only be verified when the design has been refined down to the physical level. The final verification of the design is shown as constraint verification in Fig. 1b. The functional and constraint verification are not independent and are the dominant cost components that make complex VLSI design in standard cells unaffordable.

High-level synthesis has been intensely researched for the last three decades to increase automation beyond RTL and thus reduce manual refinement. However, it is still not mainstream; as recently as 2016, the status of HLS was judged as [15]: *“Could High-Level Synthesis be the key to the next generation of EDA? As we all know, that did not happen—despite some very large investments”*. HLS, in short, is a victim of the fundamental VLSI design challenge discussed earlier. This rules out synthesis of ASIC-like custom hardware from even higher abstractions: application and system levels.

B. Synchoricity to the rescue

Synchoricity solves the challenges discussed above by borrowing two core ideas from the two previous generations of VLSI Design Style. The idea that is borrowed from the standard cells is to reduce the design space by raising the physical design to RTL, as shown in Fig. 1c. The concept of composition by abutment is borrowed from the Mead-Conway structured VLSI

design methodology for full-custom designs. Using the composition by abutment, all wires are created by abutting the RTL standard cells that we call SiLago (Silicon Lego) blocks. As a result, once the functionality is defined in terms of RTL operations exported by the SiLago blocks, the physical design of logic and also wires is known. The physical design is created by simple abutment of the SiLago blocks and without any need for logic and physical synthesis. This effectively raises the physical design to RTL for both logic and wires and has the effect of exponentially reducing the design space. as shown in Fig. 1c. Synchoricity and composition by abutment makes this reduced space predictable and composable. This empowers HLS, the synthesis from algorithms because the physical design is just one abstraction lower at RTL. This is exploited to build a library of implementations of function libraries (BLAS, LinPack, Matlab toolboxes etc.) in varying dimensions and degrees of parallelism. By building a library of standardised functions and implementations, the design space can be further reduced, as shown in Fig. 1d, and the physical design can be effectively raised to the algorithmic level. This significantly reduced design space enables automation from system and application levels. Automation has two benefits. Firstly, it enables the synthesis of custom ASIC-like design, and secondly, it provides correct-by-construction guarantee that eliminates the functional verification. The constraint verification is also eliminated because synchoricity makes the reduced design space predictable with post-layout accuracy. We refer the reader to [16] for an early version of application-level synthesis and how it differs from HLS.

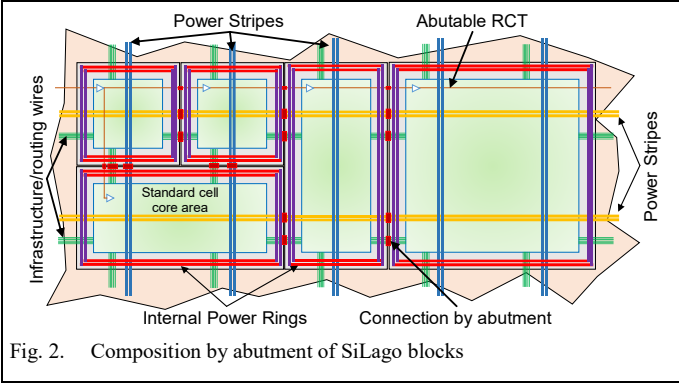
We close this section with Table I, where we compare the standard cells with the synchoros VLSI design styles and show how the former overcomes the limitations of the latter.

TABLE I
STANDARD CELLS VS SYNCHOROS DESIGN

Standard Cells	Synchoros VLSI Design
Physical design atomic building blocks	
All designs are composed in terms of Standard cells, that are atomic physical design building blocks that implement Boolean operations.	All designs are composed in terms of domain-specific SiLago blocks that are atomic physical design building blocks that implement RTL operations.
Physical Design raised to higher abstractions	
The dimension and position of every intra standard-cell wire segment is known, when the design is at the Boolean level. A follow-up physical synthesis is required to implement inter standard cell wires and buffers.	When a design is at RTL level, dimension and position of every intra and inter SiLago Block transistor and wire-segment is known. This advantage over standard cell is enabled by the Synchoricity property of the SiLago blocks.
Reduction in VLSI Design Space	
Reduces VLSI design space from $((T^L)^R)^A)^P$ to $((L^R)^A)^P$.	Reduces VLSI design space from $((T^L)^R)^A)^P$ to $(R^A)^P$.
The reduction in design space enables <i>partial</i> automation from RTL to Physical level; system-level to RTL refinement remains manual.	The reduction in design space enables <i>end-to-end</i> automation from system-level to RTL that is equivalent to being at Physical level (GDSII).

III. THE SYNCHOROUS VLSI DESIGN FRAMEWORK

In this section, we present an experimental synchoros VLSI



design framework. This framework forms the basis for arguing why a new method for RCT (Regional Clock Tree) generation by abutment is needed. Even though is not focus of this paper, all inter-SiLago wires and not just RCT are created by abutting SiLago blocks. We next briefly discuss the salient points about this experimental synchoros VLSI design framework.

A. Synchoros SiLago Blocks and Composition by Abutment

SiLago blocks are synchoros, i.e., their spatial dimensions are discrete in terms of the virtual grid cells, as shown in Fig. 4. Composition by abutment is enabled by bringing *all* the inter-SiLago block interconnects (functional and infrastructural wires like clock, power grid, etc.) to the periphery, at the right place and on the right metal layer. As a result, when functionally compatible SiLago blocks are placed on the grid, their corresponding interconnect points abut to create a larger valid VLSI design. The alignment of the interconnect points happens without any further need for VLSI engineering, other than what has already gone into creating the SiLago blocks, see Fig. 2. We note that Lego bricks are also synchoros and enable the creation of an arbitrarily complex system by abutting the Lego bricks.

B. Regions: Domain-specific SiLago Blocks

SiLago blocks are heavily customised for specific application domains called regions. There are two broad categories of regions: functional and infrastructural. Fig. 3 shows examples in these two categories. Functional region types roughly correspond to the dwarfs identified in the Berkeley Report on Landscape of Parallel Computing [17]. Functional regions are domain-specific Coarse Grain Reconfigurable Architectures (CGRAs). These CGRAs are customised for their respective domains for computation, control, address-generation, regional-interconnect, access to scratchpad etc. Differentiation of SiLago CGRAs compared to others is elaborated in [1]. Evidence of these CGRAs achieving power and performance comparable to ASICs that is typically 3-5 orders higher than GPUs is provided in [9, 11, 1].

C. The generality of synchoros VLSI design framework

Synchoros VLSI design style is as general as the standard cell-based design style. This claim is predicated on the assumption that a finite set of regions can cover the functional and infrastructural needs of any arbitrary application or system. This is also the implicit assumption in the Berkeley report [17] and the library based development environments like Matlab and Simulink. The regions listed in Fig. 3 should be sufficient for most applications and systems. We anticipate, most systems

would require multiple region instances of different types. However, should there be a domain that is not covered by the regions shown in Fig. 3a, it is not a fundamental limitation of the synchoros VLSI design style that it is not there, it is merely a question of an *extra one-time engineering effort* to create such a region. For instance, if a standard cell library lacks Mueller-C standard cell, it may be hard to implement handshake protocol. However, this is not a fundamental limitation of the standard cell-based design style. A one-time effort to design a Mueller-C standard cell would be sufficient. We also emphasise that the synchoros VLSI design style is not restricted to compile-time static data-parallel applications. We also target reactive, non-deterministically concurrent and communicating applications.

D. Three Levels of Hierarchy

In the synchoros VLSI design framework, there are three levels of hierarchy: local, regional and global, see Fig. 3b. The design of the clock distribution network is also divided into three levels, see Fig. 4. The synchoros grid in Fig. 4 enforces synchoricity. Each hierarchy level uses a different clock distribution mechanism.

Local: At the local level, i.e., the intra-SiLago block level, all wires – functional and infrastructural – are designed ad-hoc and synthesized by the commercial EDA tools. The same way they are done in standard cell-based design flows. In this case, the local clock tree (LCT) is also synthesized by the EDA tools.

Regional: Region instances are aggregation of region specific SiLago blocks. All inter-SiLago block wires in a region instance are created by abutment. SiLago blocks communicate with each other via *local region specific NOCs*, see [20-24]. Regional Clock Trees (RCT) are design constructs that are absorbed in each SiLago block. When SiLago blocks in a region instance abut, an RCT gets created that feeds the LCTs in each SiLago block by balancing the skew and in the same time maintaining the slew rate.

Global: The global level is the chip level and is composed of region instances, also composed by abutment. Region instances communicate with each other using global NOCs, see [1] for more details. These global NOCs are composed of SiLago blocks for buffered wires, NOC logic and region specific network interface units. Region instances communicate with each other on latency insensitive basis using a variant of GALS, called Globally Ratiochronous and Locally Synchronous (GRLS) method. For more details we refer the reader to [25]. The Global Clock derived from PLL(s) is distributed via the space allocated for global NOCs. It is used to feed the RCTs in each region instance via a GRLS interface at region instance

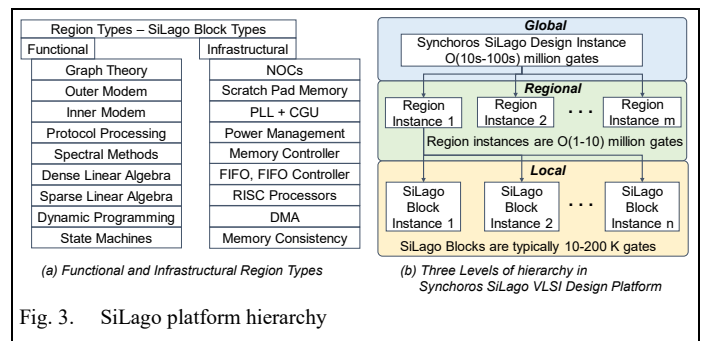


Fig. 3. SiLago platform hierarchy

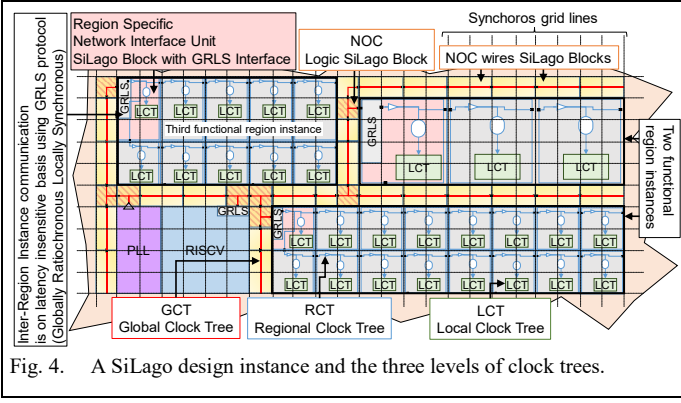


Fig. 4. A SiLago design instance and the three levels of clock trees.

boundaries. Often the GRLS interface is absorbed as part of a region specific network interface unit.

E. Overview of Synchoros VLSI Design Flow

The synchoros VLSI design flow has three components, as shown in Fig. 5. Two of these components are a one-time engineering effort, and the third component is used by the end-user. The first component is responsible for the development of the Synchoros SiLago platform. This methodology component is based on commercial EDA tools. SiLago region types are designed at RTL, verified, synthesised down to physical level, made synchoros, abutment-ready and characterised with post layout data, see [26]. The result is a library of synchoros SiLago block types, the leaf nodes in Fig. 3b. The RCT fragment in each SiLago block type is designed and incorporated during this phase, as shown in Fig. 5.

The second component develops a library of function implementations or FIMPs using SiLago HLS tool. The HLS implements each function/algorithm/actor that could be used to compose application or system models in M different architectures. Each one of these M implementations employs different degrees of parallelism, with different cost metrics (area, latency and average energy). For instance, FIMPs for 2048 point FFT actor could vary in number and type of butterflies. The libraries developed correspond to BLAS, LinPACK, Matlab toolboxes etc.

The third component transforms the application and system models composed in terms of actors/functions to custom synchoros design in terms of SiLago blocks. At present a proof-of-concept application-level synthesis tool exist, see [16] and we are in the process of enhancing it to system-level synthesis.

With the above background on the experimental synchoros VLSI design framework, we are ready to elaborate the design of the RCT fragment in SiLago blocks that enable composition by abutment.

IV. RCT BY ABUTMENT IN SYNCHOROS VLSI DESIGN

In this section, we elaborate the RCT design scheme. We first lay down the requirements of synchoros VLSI design in sub-section IV.B, with which the RCT design must comply. After the requirements, we elaborate the RCT scheme in terms of its components in sub-section IV.C. Next, in sub-section IV.D, we elaborate the delay model of the RCT that is generated as a one-time activity, as part of the design of synchoros VLSI platform. We then explain how the delay model is used during application and system-level syntheses. Finally, we present a method for

minimising the difference in the arrival of RCT in each SiLago block's LCT and present its solution in section V..

A. RCT Requirements in Synchoros VLSI Design

Regional clock tree (RCT) synthesis, like any other clock tree synthesis, has two constraints. The first is to minimise the clock skew, to maximise the percentage of clock period that can be used by the combinational logic. The second is to maintain sufficient drive strength to ensure that the slew rate, a technology-design-rule, is not violated. The latter constraint is critical because the timing models are characterised for a tight range of slew rates. If this range is violated, the timing model would no longer be valid. Finally, such a clock tree should factor in variations in manufacturing, temperature and power supply. Besides these standard requirements on RCT that all clock trees must fulfil, there are two new requirements imposed by the synchoros VLSI design. The RCT generated by abutment must additionally fulfil the following two constraints:

1) Space Invariance

All SiLago blocks of the same type should have identical electrical properties: delay, load, drive etc. This requirement stems from the need to make the cost metrics of a synchoros VLSI design predictable for the syntheses tools. A signal that propagates through a SiLago block of a specific type should have the same characteristics regardless of its location in the fabric. If this requirement is not fulfilled, the same SiLago block type would have to be characterised for each possible location in the fabric. Such an engineering effort would be unscalable.

2) No follow-up VLSI engineering after abutment

The second requirement is that when SiLago blocks abut, the RCT fragments should compose into a valid RCT tree. This should happen without having to do any further synthesis of wires, buffers or verification in terms of static timing analysis (STA) or DRC (Design Rule Check).

Fulfilling these two requirements is the key contribution of this paper. In the next sub-section, we present the RCT design scheme that achieves these requirements.

B. RCT for Synchoros VLSI Design Style

Every SiLago block has an RCT fragment that includes three components. These components enable a scalable, correct-by-construction RCT to emerge by abutment of the RCT fragments.

1) Standardised Entry and Exit Points

Every SiLago block type has standard entry (H_{in} , V_{in}) and exit (H_{out} , V_{out}) points for the RCT fragment, as shown in Fig. 6. Standard implies fixed location on specific edges and metal

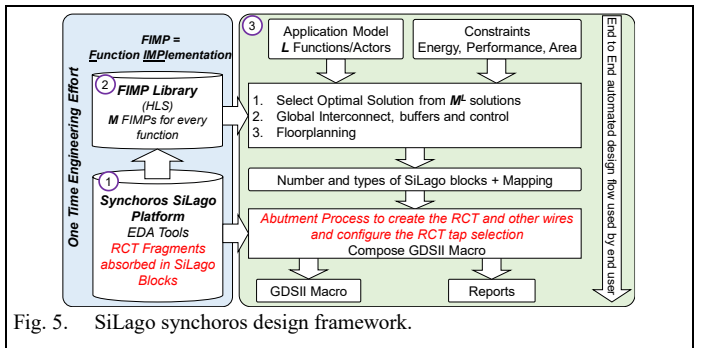


Fig. 5. SiLago synchoros design framework.

layers. The entry and exit points of RCT fragments in neighbouring SiLago blocks abut to create a valid RCT. Since the neighbours can be in horizontal, vertical, or both dimensions, SiLago blocks need entry and exit points on both horizontal and vertical edges as shown in Fig. 6.

RCT can be distributed/propagated in four orientations: top-down and left-right, top-down and right-left, bottom-up and left-right and bottom-up and right-left. The choice of orientation depends on the corner at which the GCT (Global Clock Tree) enters. The decision at which corner the GCT enters depends on the number and floor planning of the global NOCs during the application and system level syntheses decisions. As stated earlier in section II, the GCT is routed in the same physical space as the Global NOCs.

The entry point on the top-left corner of the fabric is selected to ensure that the regional clock tree can connect with the global clock tree in a regular fashion. The different SiLago blocks can vary in size, but due to synchronicity, the size is discrete and standardised, see Fig. 4. This synchronicity property of the SiLago blocks allow for blocks of different size to abut and generate a valid regional clock tree, see Fig. 2.

2) Multiplexed and buffered horizontal and vertical chords

These components have two functions. The first is to select RCT input and output, and the second is to maintain the slew rate. Selecting the input implies selecting the H_{in} or V_{in} , as shown in Fig. 6. The two inputs are fed to an OR gate. Only one of the inputs can be a clock, and the other is set to zero when configuring the RCT at the power-up time. Selecting the output implies selecting if RCT is to be propagated to the right exit (H_{out}), or the bottom exit (V_{out}), or both. The unselected exit is set to 0 not to leave any hanging wires. This is achieved using two AND gates, as shown in Fig. 6. Depending on the configuration of the two AND gates, one of the four variants of chord delay, T_{RCT_chord} gets selected, see Fig. 6. These gates also serve as the drivers to maintain the slew of the clock.

3) Programmable Delay Line

The third component is a programmable delay line that enables adjusting the delay to the LCT entry point, see Fig. 6. The delay is adjusted according to the position of the SiLago block in a region instance with respect to where the GCT enters the instance. The objective of adjusting the delay is to minimise the skew of the arrival of the RCT at the LCT entry points, in SiLago blocks in a region instance. The delay is adjusted by selecting a tap with index i in the delay line, shown in Fig. 6. The selected tap i introduces a delay t_{tap_i} between the RCT and LCT entry points.

The three components together are called *RCT fragment* and the *design* of the RCT fragments in all SiLago block types is identical. Depending on the size of the SiLago block type, the length and position of the horizontal and vertical chords, and if required the drive strength of the OR gate to maintain the slew, can differ from one SiLago block type to another. The small and simple logic in RCT fragment is built from standard cells and does not require any custom design.

The LCT (Local Clock Tree) is automatically generated by the EDA tools and can be different from one SiLago block type to another. However, all SiLago block instances of a specific type will have identical LCTs.

The RCT fragment along with the rest of the logic, wires and

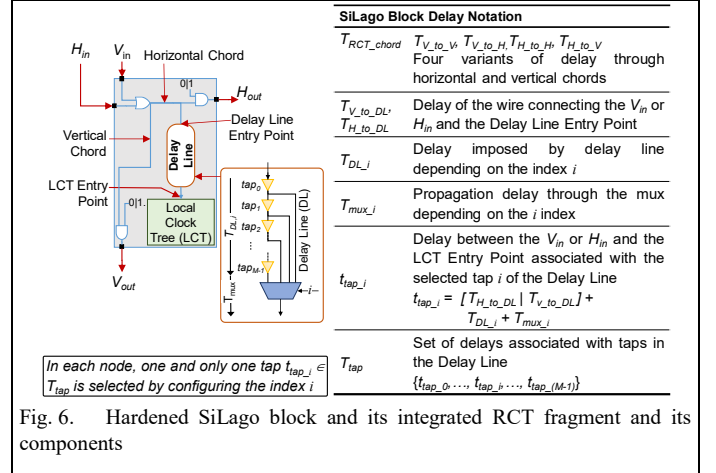


Fig. 6. Hardened SiLago block and its integrated RCT fragment and its components

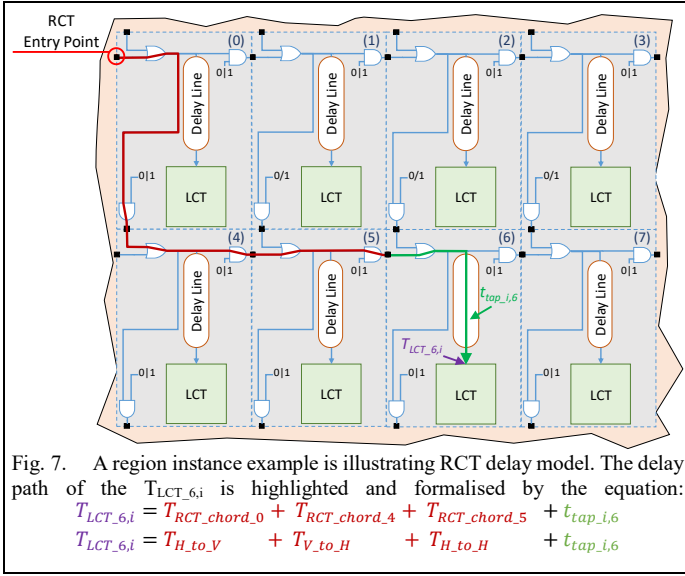
buffers in a SiLago block is hardened and characterised with post layout data. The hardening process ensures synchronicity, where SiLago blocks occupy multiples of SiLago grid cells. All interconnect wires of each SiLago block, including those for RCT fragments, are brought to the right positions and the right metal layer to enable composition by abutment. As stated, this is a one-time engineering effort and needs to be done once for each *type* of SiLago block. The hardened SiLago blocks can then be instantiated in any position in a SiLago region instance of any permissible size.

We next derive the RCT delay model that enables calculating the delay of an arbitrary RCT created by abutting the RCT fragments without having to do STA (Static Timing Analysis). This timing model is also used to decide the permissible size of a region instance and the tap index i in each SiLago block. The selection of the index i for each instance is done to minimise the skew between the arrival of RCT at LCT entry points in SiLago blocks in a region instance.

C. RCT Delay Model

The main delay that we are interested in is the latency of the regional clock tree (RCT). The RCT latency is starting from the entry point of a region instance and ends to each of the local clock tree (LCT) entry points in the SiLago blocks, see Fig. 7. There will be as many instances of this latency, as the number of SiLago blocks in the region. The notation used for this latency is $T_{LCT_x,i}$. The subscript x identifies the node id and subscript i identifies the selected tap index of the programmable delay line in node x . The purpose of the programmable line is to make all $T_{LCT_x,i}$ as equal as possible for every node x . Balancing all $T_{LCT_x,i}$ keeps the skew within the limits of the SiLago block's slack, to not cause any timing violation. $T_{LCT_x,i}$ has two components, listed below:

1. One is the sum of delays, $T_{RCT_chord}(s)$, in RCT chords in nodes that precede the node x . This delay is called the natural propagation delay of RCT, T_{nat_x} . Fig. 7 shows T_{nat_6} as the thick red line composed of RCT chords in previous nodes 0, 4 and 5.
2. The second component is the delay that is imposed on RCT by the delay line in the destination node. This *imposed* delay in the destination node n is represented by $t_{tap_i,n}$, where i is the tap index. $t_{tap_i,n}$ is itself made up of three components and defined in Fig. 6. In the example shown in Fig. 7 node 6 is the destination node and $t_{tap_i,6}$ is shown as the thick



green line.

$$T_{nat_x} = \sum_{\text{nodes previous to } x} T_{RCT_chord} \quad \text{EQ. 1}$$

$$T_{LCT_x,i} = T_{nat_x} + t_{tap_i,x} \quad \text{EQ. 2}$$

These delay components are extracted from post-layout design-data using sign-off quality timing analysis tools as a one-time engineering effort. They are space invariant, i.e., no matter where a SiLago block of a specific type is instantiated in a fabric, its delay components discussed above are the same. Note that each SiLago region type in principle contains the same type of SiLago blocks. However, there can be a small number of variants because of functional and position-dependent interconnect requirements. The SiLago blocks are characterised together with all its possible neighbours; these are typically a finite number in low tens at the most. The characterisation ensures that a valid model exists for any possible driver and load. In the experimental setup that we have used for this paper, the nodes on the edge have slightly different values of T_{RCT_chord} . These are reported in section VI.C.

The simple delay model described above can predict T_{LCT_x} with the same precision as STA applied to post-layout data. The precision is validated in section VI.D. The end-user never uses this timing model explicitly because the RCT generated is correct by construction. It is, however, used by the application and system-level synthesis tools for deciding the maximum size of the synchronous region instance and selecting the optimal number of taps in delay lines. The tap selection method is elaborated in the next section.

V. OPTIMAL TAP SELECTION IN DELAY LINES

The optimisation problem of tap selection is formulated as what is the assignment of the tap index in each node x , that would minimise the absolute difference among $T_{LCT_x,i}$. We first formulate a simpler, locally optimum cost function and then a globally optimum cost function.

To formally define these cost functions, we introduce some notations and conventions. Node IDs are $1 \dots N$ and tap indices $1 \dots M$. The first tap, $i=1$, imposes the minimum delay and the last tap, $i=M$, the maximum delay. In other words,

$t_{tap_1} = \min(t_{tap_i})$ and $t_{tap_M} = \max(t_{tap_i})$. We remind here that inside its delay line every node has the same number of taps, M . The ID of the node where RCT enters a region instance is by convention 1 and it has $T_{nat_1} = 0$ since there are no previous nodes, see 1. The node ID N is reserved for the furthest node, i.e., $T_{nat_N} = \max(T_{nat_x})$. The tap index in node N is fixed to t_{tap_1} to have minimal latency, $T_{LCT_N,1}$. This selection is made for two main reasons. The first is to minimise the insertion delay to the blocks. The second is to minimise the number of buffers used in each delay line, reducing the power consumption of the clock tree. As a result, the search space excludes the tap index space in node N , and it is fixed to 1.

A. Locally Optimum Solution

The locally optimum cost function in EQ3, L_abs_mean quantifies the mean of the absolute differences between $T_{LCT_x,i}$ and $T_{LCT_N,1}$, where $x=1 \dots N-1$.

$$L_abs_mean = \frac{1}{N-1} \sum_{x=1}^{x=N-1} |T_{LCT_x,i} - T_{LCT_N,1}| \quad \text{EQ3}$$

Since L_abs_mean is a sum of absolutes, the minimality of L_abs_mean can only be guaranteed if each term in the summation is also minimal. This, in turn, can be guaranteed by visiting each of the $1 \dots N-1$ nodes and sweeping through the M taps to find the index that gives the minimal absolute difference, with respect to the reference node N . This recipe for finding the locally minimal solution I_{LM} is formalised in 4.

$$I_{LM} = \{i \mid 1 \leq i \leq M \quad \text{AND} \quad 1 \leq x \leq N-1 \quad \text{AND} \quad T_{LCT_x,i} - T_{LCT_N,1} = \min_{1 \leq j \leq M, j \neq i} (T_{LCT_x,j} - T_{LCT_N,1})\} \quad \text{EQ4}$$

To conclude, L_abs_mean will be minimal if we replace $T_{LCT_x,i}$ with $T_{LCT_x,k}$ where $k=I_{LM}(x)$. The complexity of a locally optimum solution is $\mathcal{O}(N \cdot M)$. This is evident from the 4, where there are $N-1$ nodes to be evaluated, and in each node, there are M taps to be evaluated.

What makes L_abs_mean local is the fact that it minimises the mean with respect to a single node – the furthest node. If the reference node is changed to some other arbitrary node K , there is no guarantee that I_{LM} would give a minimal L_abs_mean . In short, L_abs_mean related to any node would prioritise the needs of a single node, potentially at the expense of other nodes.

Before we present the global cost function, we would like to complement the concepts introduced above with a concrete example. This example is then also used with the global cost function to highlight the difference.

A SiLago region instance can be modelled as a DAG

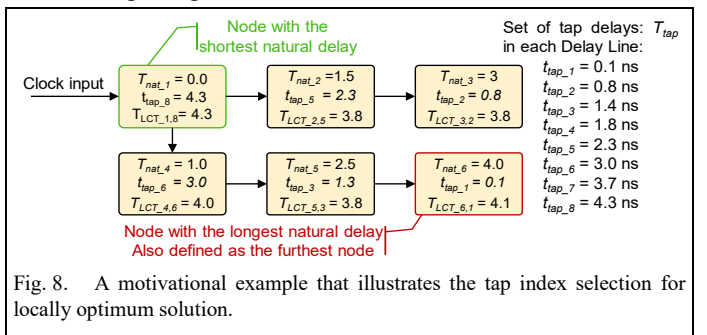


Fig. 8. A motivational example that illustrates the tap index selection for locally optimum solution.

(Directed Acyclic Graph) laid out as a two-dimensional mesh shown in Fig. 8; this example is a subset of the example shown in Fig. 7 with 6 instead of 8 nodes. Each node in the DAG represents a SiLago block, and the edge to the nearest neighbour represents T_{RCT_chord} . Without loss of generality, let us simplify the four variants of T_{RCT_chord} to two: horizontal and vertical with 1.5 and 1.0 units of delay respectively. Each node x is annotated with its node-ID and the values of delays introduced in 1 and 2. The values in the nodes reflect the assumption that the RCT enters the region instance at top-left corner and propagates in top-down, left-right fashion. Each node is equipped with a delay line with $M=8$ taps. The delay associated with each tap is shown on the right side in Fig. 8. In this example, the taps are selected to have a minimal L_abs_mean corresponding to the furthest node 6.

The equation 3 is used to calculate the L_abs_mean in the example given in Fig. 8 and is equal to:

$$L_abs_mean = \frac{1}{5} \sum_{x=1}^{x=5} |T_{LCT_x,i} - T_{LCT_6,1}| = \frac{1}{5} (0.2 + 0.3 + 0.3 + 0.1 + 0.3) = 1.2/5 = 0.24$$

B. Globally Optimum Solution

A global cost function would take into account the needs of all nodes. G_abs_mean is such a cost function and quantifies the sum of differences of $N-1$ nodes with respect to each of the N nodes as the reference; y replaces N in 3 and is swept over $1 \dots N$, EQ. 5.

$$G_abs_mean = \frac{1}{N(N-1)} \sum_{y=1}^{y=N} \sum_{x=1, x \neq y}^{x=N-1, x \neq y} |T_{LCT_i,x} - T_{LCT_i,y}| \quad \text{EQ5}$$

The global nature of G_abs_mean implies that it is no longer sufficient to select tap index in each node *independently* of the tap index selection in other nodes. Since there are N nodes and each node has M taps, there are M^N possible configurations of the delay lines, I_{conf} , in a region instance:

$$I_{conf} = \{I_1, I_2 \dots I_k \dots I_{M^N}\} \text{ where } I_k = (i_1, i_2 \dots i_x \dots i_N) \text{ and } i_x \in \{1, 2 \dots M\}$$

Note that I_k is a sequence and not a set; the elements of this sequence i) have an order $1 \dots N$ and ii) can have duplicates. Next, we define $G_abs_mean(I_k)$ for the candidate solution I_k :

$$G_abs_mean(I_k) = \frac{1}{N(N-1)} \sum_{y=1}^{y=N} \sum_{x=1, x \neq y}^{x=N-1, x \neq y} |T_{LCT_ix,x} - T_{LCT_iy,y}|$$

where $ix = I_k(x)$ and $iy = I_k(y)$

The globally minimal solution I_{GM} is then defined as follows:

$$G_abs_mean(I_{GM}) = \min_{I_k \in I_{conf}} G_abs_mean(I_k)$$

We next apply the above recipe for finding the globally optimal solution for the same problem that was used in the previous section. We have plotted all 8^5 different solutions in the globally optimum search space, Fig. 9. The green circle identifies the globally minimal solution: $I = \{7, 5, 2, 6, 3, 1\}$ and absolute variation 0.173 . When the tap selection, in Fig. 8, that was made for minimal L_abs_mean is used to compute the G_abs_mean , it will result in $G_abs_mean = 0.24$. The result proves the benefit of adopting G_abs_mean as the cost function.

The globally optimal solution has an exponential complexity of $O(N^2 \cdot M^N)$. The N^2 factor represents the complexity of

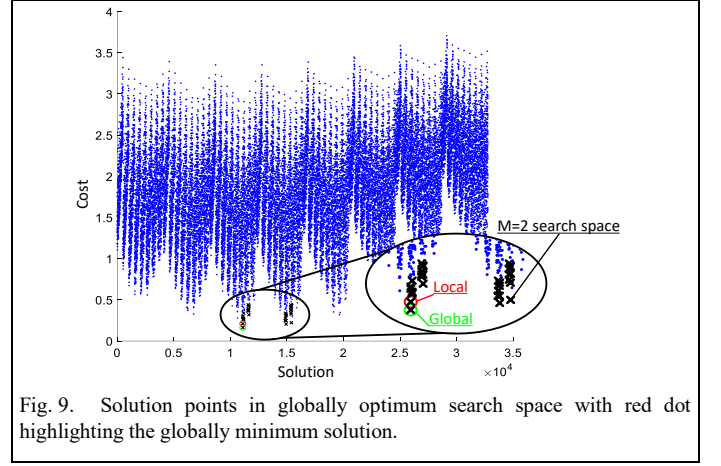


Fig. 9. Solution points in globally optimum search space with red dot highlighting the globally minimum solution.

calculating the cost-function. In the experimental platform, we report in section VI, $M=32$. Even for a small region instance of just ten nodes, the complexity is of the order of $\sim 10^{17}$ evaluations of abs differences. Fortunately, this design space can be easily pruned down to a scalable size without sacrificing the global optimality. We next justify how M can be pruned down to 2, i.e. $M=2$ independent of the dimension M of the delay line. We also motivate why we can replace N with N' , where $N' \ll N$ and N' is independent of the size N of region instance.

C. Pruning the Search Space of the delay-line tap selection

In this section, we justify the basis for dramatically pruning the configuration space.

1) Justifying $M=2$

Ideally, we would like L_abs_mean and G_abs_mean to be zero. Since these cost functions are the mean of absolute differences, in order for them to be zero, each term should be reduced to zero. This, in turn, requires the two T_{LCT} terms in absolute difference expression to be equal. Since T_{nat} component in T_{LCT} is invariant, the t_{tap} should have an exact delay to make the two T_{LCT} equal. This delay is called the ideal t_{tap} delay. For the L_abs_mean case, this is formalised as follows in EQ 6.

$$t_{tap_ideal,x} = T_{LCT_N,1} - T_{nat_x} \quad \text{EQ6}$$

Such an ideal tap delay is not possible in practice because it requires an infinitely divisible delay line. However, the ideal tap delay helps identify the *two* contiguous tap indices whose delays bracket the ideal tap delay. This is illustrated in Fig. 10 and as can be seen, t_{tap_ideal} is the basis for finding the two taps i and $i+1$ whose delay brackets the t_{tap_ideal} in node x . We can repeat this process for all $N-1$ nodes. As a result, the lower and upper bound taps i and $i+1$ for each node will be identified. As

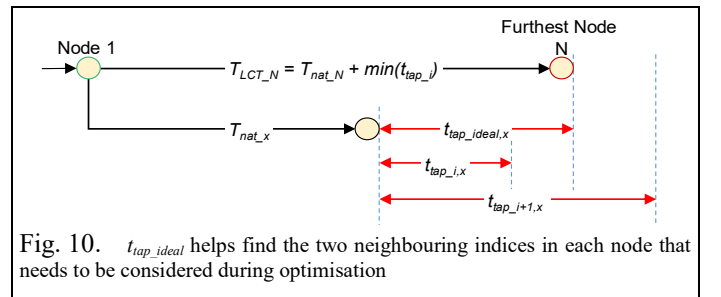


Fig. 10. t_{tap_ideal} helps find the two neighbouring indices in each node that needs to be considered during optimisation

stated before, the node N has a pre-decided tap index to minimise the propagation delay of the clock and allow the larger possible size for a region. We represent this sequence of ideal lower bound indices by $Ideal_LB$. By knowing the lower bound index $i = Ideal_LB(x)$, we can easily compute the ideal upper bound index to be $i+1$.

The above justification is done for L_abs_mean that uses the furthest node as the reference. For G_abs_mean , we still maintain the assumption of the furthest node N having a fixed tap index set to $\min(t_{tap,i})$. This assumption allows us to retain the same index bounds as LB_ideal for $1 \dots N-1$ nodes while searching for the globally optimal solution. Note that this does not in any way compromise the global optimality.

In conclusion, the complexity reduces to $O(2 \cdot N)$ and $O(N^2 \cdot 2^N)$ for locally and globally optimum solutions, respectively. 2^N is still a large factor, and we next justify why this can be pruned down by replacing N by $N' \ll N$.

2) Justifying $N' \ll N$

A combinational path implies a register output to a register input path, that is composed of wires and combinational logic. The clock skew between such register to register paths should be minimised. The cost functions specified in EQ3 and EQ4 attempt to minimise such skews, i.e., the absolute difference in T_{LCT} between the furthest node pairs (like 1 and N) and between the nearest neighbours. Such optimisation would be necessary if every node pair in a region instance is connected by a combinational path. This is not the case and is the basis for replacing N by $N' \ll N$.

To understand this, let us revisit the local NOCs: the intra-region-instance, structured interconnect scheme in synchoros VLSI region types, see section III. These local NOCs serve two purposes. The first is conventional; to allow SiLago blocks in a region instance to communicate with each other. The second embodies the spirit of Synchoricity and allows the functionality hosted by individual SiLago blocks to be clustered to provide variations in function, capacity and degree of parallelism. Standard-cell-based VLSI design achieves this objective by synthesising ad-hoc wires to cluster the standard cells. In synchoros VLSI design, these wires pre-exist as fragments of local NOCs in SiLago blocks. The region-wide local NOCs emerge as a result of the abutment. However, in synchoros VLSI design, the combinational paths between SiLago blocks are restricted to a small window. The window slides by a certain stride to cover the entire region instance, as shown in Fig. 11. This structure implies that two SiLago blocks that are located in different windows do not have any combinational path between them. As such, there is no need to worry about clock skew between them. Communication between such SiLago blocks is possible but involves multiple hops/cycles, i.e., the path is pipelined.

Since every node is not connected to every other node but only to nodes surrounding it in a sliding window, the problem can be simplified. The absolute difference in arrival time that RCT needs to minimise is between every node x and a small set of nodes surrounding it in a sliding window. The nodes inside the sliding window are combinational reachable from x . In the example shown in Fig. 11, this small set of nodes $N'=15$. In the synchoros VLSI region type called DRRA, $N'=14$, see [27].

The space invariance property might suggest that once the

absolute difference has been minimised for one sliding window, the same solution should apply to all others. Unfortunately, this is not true. If the overlap between sliding windows is zero, the solution for one sliding window will apply to all others. Because of the overlap, the natural delay of RCT, though perfectly predictable, is not uniform. Finally, the size of the sliding window decides N' and is evident from example in Fig. 11, it is independent of the size of the region instance.

D. Maximum Size of Region Instance

The timing model parameters that were introduced in section IV.C are also used to decide the maximum size of region instance that is allowed during the system-level synthesis. We remind the reader that region instances are treated as synchronous regions. More accurately, the clocks of all the flops within a region instance are phase-aligned but not necessarily skew aligned. Paths within the sliding window span are skew aligned. Since the sliding windows overlap, all flops in a region instance have a phase-aligned clock even if there is no timing path between them, as shown in Fig. 11. A concrete manifestation of this policy is that the furthest node has the smallest tap delay assigned to it, and this is not subject to change as part of optimization. The fixed tap selection of the furthest node, not only guarantees minimal RCT latency to the furthest flops, but also decides the maximal logical span of region instance. In essence, the number of taps and their ability to compensate the monotonous increase in $T_{nat,x}$ with tap delays dictates the maximum size of region instance allowed.

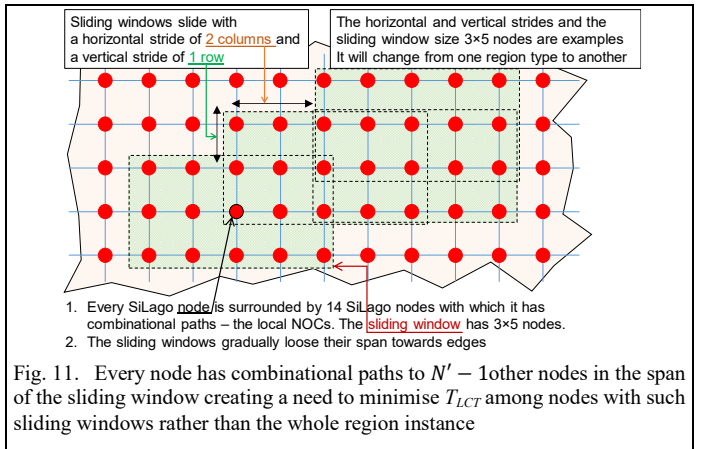
$$\max(t_{tap,i}) - \min(t_{tap,i}) \leq \max(T_{nat,x})$$

We quantify the above equation in the next section and also show how the region instance size scales with the number of taps.

VI. EXPERIMENTS AND RESULTS

In this section, we experimentally validate the key claims of the ability to generate a valid and predictable RCT by abutment with the end-user not having to do logic or physical synthesis. A valid RCT means that the generated RCT is guaranteed to be timing and DRC (Design Rule Check) clean. A predictable RCT means that all properties of the generated RCT are known with post layout accuracy without having to do Static Timing Analysis.

Three experiments were performed. The first experiment reports the results of the RCT model and its properties, as



discussed in the section IV.D. The second experiment then uses the RCT model to predict the properties of the RCT in an experimental design. The predicted values are validated against the values analysed by commercial EDA tools. A side effect of this experiment is that RCT generated by abutment is shown to be timing and DRC clean by the commercial EDA tools. The third experiment benchmarks the properties of RCT generated by abutment against a functionally equivalent RCT, generated by the EDA tools. The results of the experiment are used to prove that the two clock trees are comparable in their figures of merits. That is to say that the synchronicity and abutment does not degrade the quality of the generated RCT.

A. Experimental setup

In this sub-section, we present the experimental setup we have used for our experiments.

1) Technology and Tools

All experiments have been implemented in 40 nm technology node and the results have been validated using commercial EDA tools. These tools have been used for three purposes:

- To build the synchronos VLSI design platform, including RCT design and its characterisation. This use of EDA tools is a one-time engineering effort, and it is not seen by the end-user.
- To validate the claim that the generated RCT is timing and DRC clean and predictable.
- To demonstrate that the benefits of synchronicity and abutment do not degrade the quality of RCT.

2) Experimental Design

The proposed RCT by abutment scheme and the state-of-the-art hierarchical EDA flow are applied to the same experimental design. The design is a composite region instance of two different types. The two types are a dense linear algebra CGRA fabric called Dynamically Reconfigurable Resource Array (DRRA) [20] and a CGRA for scratchpad fabric called Distributed Memory Architecture (DiMArch) [22].

The region instance has 24 SiLago blocks that correspond to roughly 1.5 million NAND gates and 16 kBs of SRAM, or 4 mm² in 40 nm. The size of the design is compatible with the expected typical size of synchronous region instance, for which the RCT is generated by abutment. To establish the scalability of the method, we also show the results of a 5 million gate design and show that the predictability is unaffected.

B. RCT Model

An RCT fragment, shown in Fig. 6, with 32 taps in delay line was incorporated into the DRRA and DiMArch SiLago blocks. These blocks were hardened to be synchronos, and all interconnects, including the RCT interconnects, were brought to the periphery to enable abutment, conceptually shown in Fig. 12. The RCT model parameters were extracted using STA (Static Timing Analysis) from the post layout data and results tabulated in Table II. The SiLago blocks on the edges have slightly different values of T_{RCT_chord} compared to the ones in the middle. Because there are minor differences in the interconnect and the layout of the three rows in Fig. 12, each row has different T_{RCT_chord} delays. The delay model takes that into consideration to correctly predict the T_{nat} . Here we report the values for the middle row. The slew at LCT entry point and the total capacitance of the RCT structure in each SiLago block is

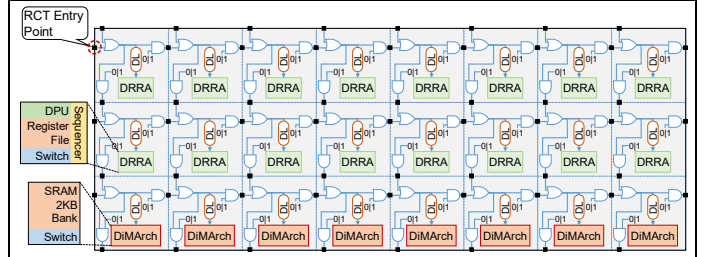


Fig. 12. Experimental Region Instance used in Experiments.

reported as well. The tap delay t_{tap_i} in our setup can introduce delay from 1.7 to 6.2 ns.

The timing model created above factors in variations in temperature, VDD and process as part of standard logic synthesis. For the experiments reported in this paper, the timing model takes into account the Best and the Worst Case Commercial variations. *The multi-corner analysis ensures that the RCT constructs, along with its timing and electrical properties, will have the robustness that has been factored in these variations.*

TABLE II
RCT MODEL'S PARAMETER VALUES

Parameter	Value	Parameter	Value
T_{RCT_chord}	$T_{H_to_H}$	$T_{V_to_H}$	0.617ns
			0.663ns
	$T_{H_to_V}$	$T_{V_to_V}$	0.618ns
			0.646ns
Slew at LCT entry			67ps

C. Predictability and validity

The RCT model quantified in the previous sub-section was used to predict the properties of the RCT created by abutment, as shown in Fig. 12. The prediction is done by taking the post layout SiLago region instance created by abutment and analysing the properties of the generated RCT by two methods, as shown in Fig. 13. The first method is to use the RCT model and SiLago analysis scripts embodied by equations 1 and 2. The second method is to use EDA analysis tools. The results of these paths are compared to establish the accuracy of the RCT model with EDA tools as the benchmark. A side-effect of this experiment is that the RCT created by abutment gets certified as being timing and DRC clean by the EDA analysis tools.

The two RCT properties that we focus on predicting are the arrival times of RCT, $T_{LCT_x,i}$, and the slew rate at the entry point of LCT in each of the 24 SiLago blocks. A third property we predict is the combined capacitance of the RCT structure in 24 blocks. The optimisation algorithm described in section V.C was used to find the optimal set of tap indices in the 24 blocks

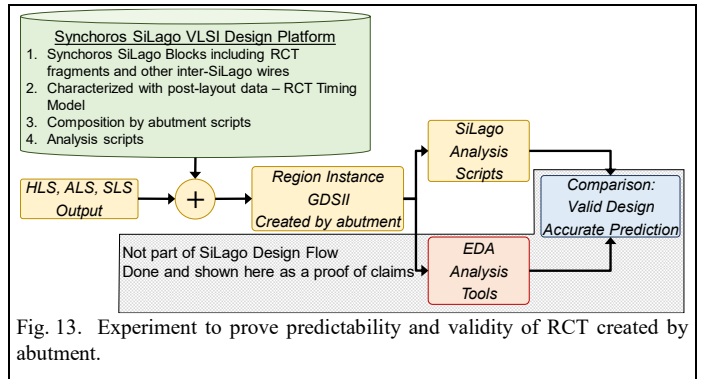


Fig. 13. Experiment to prove predictability and validity of RCT created by abutment.

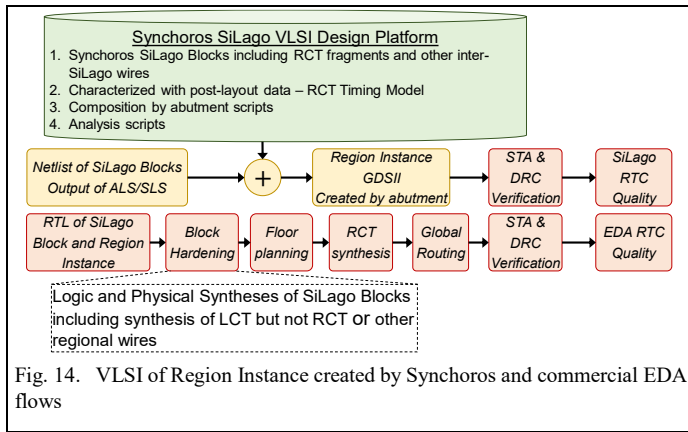


Fig. 14. VLSI of Region Instance created by Synchoros and commercial EDA flows

to minimise the absolute difference among $T_{LCT, x, i}$. Two critical quantified conclusions can be drawn. The first is that the worst-case absolute difference is 129 ps which is easily absorbed by the slack margin with which the SiLago blocks are synthesised. The second is that the predicted values by the SiLago Analysis Tools are almost identical to the one analysed by the EDA tools. The worst-case error compared to EDA tools is 1.5 ps, and the RMS is 0.0005ps. We believe that this difference comes from the fact that our experimental setup does not have an infinite ground plane. This results in different parts of the design experiencing different coupling with long signals, like the reset, and the ground plane. The resulting model suffices as a proof of concept and provides sufficient accuracy that a post abutment STA is not needed.

The slew rate at each LCT entry point and the total capacitance predicted by both methods are a near-perfect match between SiLago and EDA tools. The SiLago design reports slew and capacitance equal to 67ps and 129.9pf. The EDA respective values are 87ps and 127.2pf. We want to note here that this is the capacitance for the whole clock in the region composed of RCT and LCT. LCT dominates the percentage capacitance with 97% capacitance, while the RCT has just 3%.

To address scalability concerns, we first performed the experiments, as reported above, using a baseline design of eight columns and three rows. The baseline design corresponds to ~ 1.5 million gate. Then we repeated the experiment for a larger design with twenty-five columns and three rows corresponding to roughly 5 million gates. The predictability of the larger design was as good as the one of the smaller design.

D. SiLago RCT comparison with EDA

In this section, we demonstrate that the quality of RCT (Regional Clock Tree) generated by abutment is comparable to a functionally equivalent RCT generated as part of a hierarchical EDA flow. This experiment is visualized in Fig. 14. The Synchoros SiLago design flow starts with an untimed model at application/system-level. Application/System-level synthesis then transforms the model into a logical netlist of SiLago blocks – the region-instance; in the current context, a single region instance¹ shown in Fig. 12. The SiLago blocks in the netlist are picked from the Synchoros SiLago VLSI design platform. The VLSI design, including RCT, of the region instance, is created by abutment. Note that the creation of the

synchoros VLSI design platform is a one-time engineering effort, like the standard cell library creation.

The second path is based on commercial hierarchical EDA flow. It starts with a logical netlist of RTL SiLago blocks that do not include the regional (inter-SiLago block) wires like RCT. SiLago blocks are hardened but do not include global wires. Once hardened, these blocks are floor-planned and the regional clock tree and inter-SiLago block wire have to be synthesized. This is done with the physical synthesis step that follows the floorplanning and generates the functionally equivalent RCT tree. Note that in EDA terminology, the RCT and inter-SiLago block wires are called global wires. We refrain from using the term global to maintain consistency with the SiLago flow, where global implies inter-region instance wires.

Both designs are then analysed by the commercial EDA tools to compare the properties of the two functionally equivalent RCTs. The results are shown in Table III. As can be seen, the values of critical parameters are comparable. The standard cell area refers to standard cells dedicated to creation of RCT, including MUX/AND/OR gates as reported from the EDA tools. In SiLago case, each SiLago block has a fixed overhead, and not all of it is used. This is the key reason for a larger overhead compared to the EDA RCT. However, do note that the RCT area as a percentage of SiLago block takes up only 0.1%.

The SiLago RCT achieves comparable arrival time of RCT at LCT (Local Clock Tree) entry points compared to the commercial EDA RCT. The SiLago RCT has slightly better slew rate at LCT entry. The average and absolute difference in slew at different points in trunks for the entire (RCT+LCT) clock tree is also comparable and within the limits of the technology rules.

TABLE III
EDA RCT vs SiLago RCT

	SiLago RCT	EDA RCT
Wire Length	422932.1 μm	415263.9 μm
Standard Cell Area	19472.6 μm^2	18276.5 μm^2
Average Trunk Slew	0.062 ns	0.090 ns
Total Capacitance	129.9pf	127.2 pf
Avg. Diff. in Arrival Time (LCT Entry Point)	0.04299ns	0.0337 ns

The above experiment and the reported results establishes that RCT generated by abutment has comparable quality as the one generated by commercial EDA tools. The difference is that the EDA tool generated RCT is ad-hoc and *synthesised anew for each design instance*. Notice that the EDA RCT's irregularity in Fig. 15a resulting from the attempt to factor and reuse the buffers. In contrast, the synchoros RCT is regular. The ad-hoc nature of the EDA RCT and its irregularity violates the requirements that synchoros VLSI design places on RCT.

The synchoros RCT by abutment is regular, as shown in Fig. 15b. It has three main branches corresponding to two DRRA and one DiMarch rows. Each branch has eight leaf nodes, and each leaf node has the same RCT structure. The regularity of the SiLago RCT enables abutment. Its regular structure, together with its absorption in the SiLago blocks as a pre-synthesized and characterised structure, enables predictability.

Though not the most critical difference, the RCT generated by commercial EDA tools took ~ 50 minutes for synthesis and

¹ In general, ALS and SLS will output multiple region-instances connected by global NOCs and communicate on latency insensitive basis using GRLS [25].

In this paper and experiment, we focus on RCT generation by abutment in a single region instance. The same process would apply to all region-instances.

another ~ 5 minutes for STA, for a modest 1.5 million gate design. Any post-CTS optimisation requires another ~ 30 min. This time is expected to increase exponentially with design size. In the case of synchoros RCT, the clock tree generation and its analysis are instantaneous.

VII. STATE OF THE ART

In this section, we justify the contributions of this paper in comparison to the state-of-the-art, primarily in clock tree synthesis but also in composition by abutment.

CTS (Clock Tree Synthesis) has been researched since the earliest days of VLSI. One of the most critical chapters in the classic textbook on VLSI Systems by Mead-Conway [14] is dedicated to clocking and timing. Ever since then, CTS has been a mainstream VLSI research topic. The main objective of CTS research has been to optimise the cost metrics of the clock tree, i.e., smaller switching capacitance, minimising skew, maintaining edge etc. [28, 29]. These approaches are based on sophisticated heuristic algorithms. Most of these methods are based on the van Ginneken dynamic programming algorithm for buffer insertion and sizing, and the delay model used is the Elmore delay model [30]. An excellent survey of CTS techniques is presented in [31]. Additionally, they propose their own algorithm for chip-level clock tree synthesis that minimises the skew and is manufacturing variation aware. [32, 33] also propose solutions to chip-level clock tree synthesis that is aware of on-chip variations. J. Lu et al. in [34] address a different problem with a similar method, where they use a post-clock-tree-synthesis optimisation to improve the clock period. The proposed method addresses the problem by buffering an already synthesized clock tree. They are considering the synthesised local clock tree and the delay of the logic path, allowing for non-zero skew. In contrast, our goal is not to optimise the clock period, but to balance the arrival time of the clock at the source points of the local clock trees. The balance of the RCT is done by configuring an existing delay line that has already been implemented. In synchoros VLSI design style, once a SiLago block has been designed, no further change is possible and no additional external circuitry can be added.

With dynamic voltage frequency scaling becoming mainstream, research in clock tree also addressed concerns raised by varying VDD. Any variation in VDD changes the drive and thus influences the amount of skew. A common method to address this problem is the use of Adjustable Delay Buffers (ADB). There have been many research work recently that addresses this problem using ADBs [35 - 37].

H-tree and Mesh clock structures have also been widely researched [30, 38]. The regularity of these structures makes them a good match for the synchoros VLSI design style. However, both these structures do not fulfil the requirements that RCT by abutment has as part of synchoros VLSI design style. H-Tree is a hierarchical structure, and its depth would depend on the size of the region instance. For this reason, absorbing an H-Tree as RCT fragments and being able to create an arbitrary H-Tree by abutment that is depended on the size and shape of region instance is not feasible. Mesh-based clock tree poses a challenge in terms of the predictability requirement. Since the entry point in clock tree mesh, an equipotential surface, is not known, it creates cyclic graphs that are

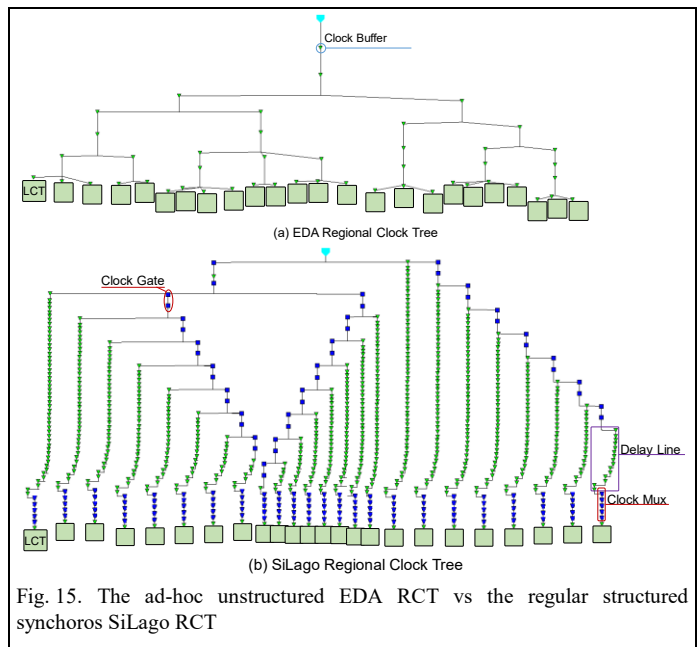


Fig. 15. The ad-hoc unstructured EDA RCT vs the regular structured synchoros SiLago RCT

impossible to analyse with STA [30, 38]. This is an even bigger problem for the RCT by abutment scheme because it requires no STA. Because of that, it is required to have iron-clad timing models that can predict the properties of RCT with sufficient accuracy. However, we note that in terms of geometry, the proposed RCT structure is a mesh structure, in which the entry point and propagation of RCT is known. The standardised entry points and propagation path makes it analysable and possible to create the RCT model, as shown in section IV.D. .

FPGAs, like synchoros VLSI designs, are regular structures and naturally invite comparison of their clock tree schemes. The fundamental difference in regularity is that the regularity of FPGAs is not modifiable in silicon for the end user. In other words, no matter how the end user configures an FPGA, the clock tree wires will not change in their position, length or drive. These wires can be configured differently but the silicon will not change. In contrast, depending on functionality and constraints, the output of application and system-level synthesis will imply different RCT wires in silicon. All of the wires are regular and structured but connected in such a way to produce different structures. FPGAs partition their leaf nodes – the flops – into clusters based on spatial locality. These clusters can be clocked by different global clock tree wires in a configurable manner. Further, depending on the datapath created by the end-user and the choice of the clock to drive them, FPGAs do require an STA as a post-synthesis step. In synchoros VLSI design, unlike FPGAs, the datapath is highly customised for a specific application domain – much more than DSP slices in FPGAs. These regions are pre-characterized to work at certain clock speeds, as long as RCT infrastructure can deliver RCT to the LCT entry points within a known skew margin. This is the reason why in synchoros VLSI design, no STA is required as a follow-up step and region instances of arbitrary size that are hosting arbitrary domain-specific functionality are guaranteed to be correct-by-construction.

The clock tree synthesis research that we address in this paper does not compete directly with these approaches. The method reported in this paper complements and builds on

existing research. As shown by our experiments and would be evident to most practitioners of VLSI design, LCT has the dominant switching capacitance. For that reason, we rely on the existing body of research to automate this step. What we propose is an alternative to the clock tree generation at a higher level, which has relatively insignificant capacitance but profoundly affects the engineering cost.

The proposed solution most directly competes against the widely prevalent hierarchical synthesis flow of the EDA tools and their global clock tree synthesis phase. We propose to replace this ad-hoc follow-up synthesis step with a one-time engineering effort. That makes the generation of VLSI design alternatives non-incrementally faster, easier and most critically predictable and correct by construction. We believe this is essential to automate the higher abstraction synthesis (see Fig. 1) as argued by Hemani et al. in [1].

Besides the RCT synthesis, another aspect of research that is proposed in this paper is the composition by abutment. Once again, this method is also as old as the VLSI designs. The Mead-Conway [14] method involved composing macros by abutting bit slices. Later, these macros were parametrised, and complete system-level design was attempted as part of silicon compiler research. This phase of VLSI design automation was eclipsed when standard cells were introduced, and composition by abutment as a method lost its appeal. More recently, [39, 40] have proposed methods that bear some similarity to the SiLago method. The proposed method does not detail how they propose to handle the synthesis of infrastructural wires like clocks, resets and power grid by abutment. The critical difference that the SiLago method has is that it aims at automating the synthesis of functional hardware. Whereas, [39, 40] aim at incrementally improving the EDA tool's hierarchical synthesis flow for designing processor centric infrastructural hardware.

VIII. CONCLUSION AND FUTURE WORK

We have presented a regional clock tree synthesis method based on abutting identical fragments of the clock tree. The fragments are absorbed in the one-time VLSI engineered abutable SiLago blocks. The generated clock tree is shown to be valid, i.e. timing clean, comparable in its cost metrics to a functionally equivalent clock tree generated by the EDA tools. The advantage that the proposed scheme has over the conventional EDA based method is that it generates a predictable and correct by construction design of the regional clock tree. Besides that, the proposed method does not require a clock tree synthesis step for the generation of the RCT. We argue that this is essential to enable automation of functional hardware from higher abstractions. We have shown that the scheme is scalable to larger designs of ~ 5 million gate complexity and the synthesis time required is less than a minute.

The programmable delay line is constructed from qualified standard cells, and its atomic delay decides the resolution to which we can minimise the skew. We are working on a more advanced programmable delay line that will allow a finer adjustment of delay that would be needed for higher frequencies. In this improved delay line, the number of taps would increase logarithmically with the amount of delay. Thereby the size of design over which it can maintain synchronicity would be increased. Such a delay line will be

constructed with weighted positional taps much like a fixed-point number. We are also in the process of making the delay of each tap in the delay line adaptive. That will allow it to be adjusted in response to changes in V_{dd} as part of dynamic voltage frequency scaling scheme.

ACKNOWLEDGEMENT

This work is supported by Vinnova, Sweden as part of the CREST II project.

REFERENCES

- [1] A Hemani, S.M.A.H Jafri, S Masoumian, "Synchoricity and NOCs could make Billion Gate Custom Hardware Centric SOCs Affordable," International Symposium NOCS, 2017.
- [2] W. J. Dally, et al., "Efficient embedded computing," *Computer*, vol. 41, 2008.
- [3] J. Rabaey, "Silicon Platforms for the Next-Generation Wireless Systems." Tutorial in *HotChips 13*, 2001.
- [4] E. S. Chung, et al., "Single-chip heterogeneous computing: Does the future include custom logic, FPGAs, and GPGPUs?," in *MICRO 2010*.
- [5] M. Khazraee, L. V. Gutierrez, I. Magaki, and M. B. Taylor, "Specializing a Planet's Computation: ASIC Clouds," *IEEE Micro*, vol. 37, no. 3, 2017.
- [6] N. P. Jouppi, et al., "In - Datacenter Performance Analysis of a Tensor Processing Unit," in *Proceedings of ISCA '17*, 2017.
- [7] S. Hanley, "Autonomous Cars Have Shorter Range Due To High Power Consumption By Computers," *CleanTechnica*, 13-Oct-2017.
- [8] K. Freund, "Will ASIC Chips Become The Next Big Thing In AI?," *Forbes*, 04-Aug-2017.
- [9] S. M. A. H. Jafri, A. Hemani, K. Paul, and N. Abbas, "MOCHA: Morphable Locality and Compression Aware Architecture for Convolutional Neural Networks," in *Proceedings of the IPDPS*, 2017.
- [10] Y. H. Chen, et al., "Eyeriss: A Spatial Architecture for Energy-Efficient Dataflow for Convolutional Neural Networks," *ISCA 2016*.
- [11] Y. Yang, et al., "RiBoSOM : Rapid Bacterial Genome Identification Using Self-Organizing Map implemented on the Synchoros SiLago Platform," in *Proceedings of the SAMOS*, 2018.
- [12] R. Merritt, "FPGAs add comms cores amid ASIC debate," *EE Times*, 03-Nov-2013.
- [13] D. Stathis, et al. "eBrainII: A 3 kW Realtime Custom 3D DRAM integrated ASIC implementation of a Biologically Plausible Model of a Human Scale Cortex." *arXiv preprint arXiv:1911.00889* (2019).
- [14] Carver A Mead, Lynn A Conway, "Introduction To VLSI Systems", Addison-Wesley. ISBN-13: 978-0201043587.
- [15] B. Bailey, "ESL Flow Is Dead," *Semiconductor Engineering*, April 28, 2016.
- [16] S. Li, N. Farahini, A. Hemani, K. Rosvall, I. Sander, "System Level Synthesis of Hardware for DSP Applications Using Pre-Characterized Function Implementations," *Proceedings of the ISSS Codes 2013*.
- [17] A. Krste, et al., "The Landscape of Parallel Computing Research: A View from Berkeley," EECS Department, UC, Berkeley, 2006.
- [18] T. Miyamori and K. Olukotun, "Remarc: Reconfigurable multimedia array coprocessor," *IEICE Trans. Inf. Syst.*, vol. E82-D, no. 2, 1998.
- [19] P. M. Heysters, G. J. M. Smit, and E. Molenkamp, "Energy-efficiency of the Montium reconfigurable tile processor," in *Proceedings of the ERSAs '04*, 2004.
- [20] M. A. Shami and A. Hemani, "Control scheme for a CGRA," *Proceedings of the SBAC-PAD*, 2010.
- [21] M. A. Shami and A. Hemani, "Address generation scheme for a coarse grain reconfigurable architecture," in *Proceedings of the ASAP*, 2011.
- [22] M. A. Tajammul, M. A. Shami, A. Hemani, and S. Moorthi, "A NoC based distributed memory architecture with programmable and partitionable capabilities," in *28th North Chip Conference*, 2010.
- [23] P. Liu, F. O. Ebrahim, A. Hemani, and K. Paul, "A coarse-grained reconfigurable processor for sequencing and phylogenetic algorithms in bioinformatics," in *Proceedings - ReConFig 2011*.

- [24] M. Badawi, Z. Lu, and A. Hemani, "Service-Guaranteed Multi-port Packet Memory for Parallel Protocol Processing Architecture," in Proceedings - 24th Euromicro International Conference PDP 2016.
- [25] J.-M. Chabloz and A. Hemani, A., "Low-Latency Maximal-Throughput Communication Interfaces for Rationally Related Clock Domains," IEEE TVLSI, vol.22, no.3, pp.641,654, March 2014.
- [26] S. M. A. H. Jafri, N. Farahini and A. Hemani, "SiLago-CoG: Coarse-Grained Grid-Based Design for Near Tape-Out Power Estimation Accuracy at High Level," 2017 ISVLSI, Bochum, 2017.
- [27] M. A. Shami and A. Hemani, "Partially reconfigurable interconnection network for dynamically reprogrammable resource array," Proceedings 2009 8th IEEE International Conference on ASIC, 2009.
- [28] T. H. Chao, et al., "Zero Skew Clock Routing with Minimum Wirelength," IEEE Trans. Circuits Syst. II Analog Digit. Signal Process., vol. 39, no. 11, 1992.
- [29] P. J. Restle et al., "A clock distribution network for microprocessors," in 2000 Symposium on VLSI Circuits Digest of Technical Papers, 2000.
- [30] L. Lavagno, I. L. Markov, G. Martin, and L. K. Scheffer, "Clock Design and Synthesis" in Electronic Design Automation for IC Implementation, Circuit Design, and Process Technology, CRC Press, US.
- [31] A. Rajaram, and D. Z. Pan, "Robust Chip-Level Clock Tree Synthesis", IEEE TCAD, June 2011.
- [32] T. J. Wang, S. H. Huang, W. K. Cheng, and Y. C. Chou, "Top-level activity-driven clock tree synthesis with clock skew variation considered," in Proceedings - IEEE International Symposium on Circuits and Systems, 2016.
- [33] C. Deng, Y. Cai, and Q. Zhou, "Fast synthesis of low power clock trees based on register clustering," in Proceedings - International Symposium on Quality Electronic Design, ISQED, 2015.
- [34] J. Lu and B. Taskin, "Post-CTS clock skew scheduling with limited delay buffering," in Midwest Symposium on Circuits and Systems, 2009.
- [35] J. Kim, and T. Kim, "Adjustable Delay Buffer Allocation under Useful Clock Skew Scheduling", IEEE TCAD Vol 36, No 4, April 2017.
- [36] K. Park, G. Kim, and T. Kim, "Mixed Allocation of Adjustable Delay Buffers Combined with Buffer Sizing in Clock Tree Synthesis of Multiple Power Mode Designs", vol. 1. European Design and Automation Association, 2014.
- [37] C.-C. Kao, "Clock Skew Minimization in Multiple Dynamic Supply Voltage with Adjustable Delay Buffers Restriction," J. Signal Process. Syst., vol. 79, no. 1, Apr. 2015.
- [38] A. Abdelhadi, et. al. "Timing-Driven Variation-Aware Nonuniform Clock Mesh Synthesis," in Proceedings of the 20th symposium on Great lakes symposium on VLSI, 2010.
- [39] W. J. Dally, C. Malachowsky, S. W. Keckler, "21st Century Digital Design Tools". DAC 2013.
- [40] R. Merritt, "EE Slashes CPU Design Cost: 4.5B transistor tapeout for less than \$1M," EE Times, 10-May-2016.



Dimitrios Stathis received his Diploma in Electr. & Comp. Engineering and a M.Sc. in Microelectronics and Computer Systems, both from the Democritus University of Thrace, Xanthi, Greece in 2013 and 2016 respectively. He received his second M.Sc. degree in Embedded Systems from KTH,

Stockholm, Sweden in 2017. He is currently working towards the PhD degree at the KTH, Stockholm, Sweden. His research interests include Computer Architectures and ASIC design for multimedia applications and Artificial Neural Networks.



Panagiotis Chaourani received the B.Sc. degree in Physics and the M.Sc. degree in Electronics, both from the Aristotle University of Thessaloniki, Thessaloniki, Greece in 2011 and 2014 respectively. He is currently working towards the PhD degree at the KTH, Stockholm, Sweden. His research interests include IC design, CAD tools and monolithic 3-D integration.



Dr. Syed M. A. H. Jafri is a senior system architect working at Ericsson. Before that, he worked as a post-doc researcher at the Royal Institute of Technology (KTH). He received his B.Sc. degree in 2005 from National University of Sciences and Technology in Rawalpindi, Pakistan. From 2005 to 2007 he was with Siemens, Pakistan. In 2009 he received MSc in system on chip design from Royal Institute of Technology (KTH), Sweden. He did PhD from University of Turku, Finland in 2015. He has 40+ peer-reviewed journals/conference publications.



Ahmed Hemani is Professor in the Electronics Dept. at School of EECS, KTH, Stockholm, Sweden since 2006. His doctoral thesis on HLS was the basis for one of the first commercial HLS product from CADENCE. Later he has contributed to latency insensitive design style with research on GALS and GRLS. He also pioneered the concept of NOCs. His current research interests focus on massively parallel architecture and design methods for them to achieve ASIC comparable performance. He has introduced the concept of synchronicity and driven the development of the SiLago as an experimental synchoros VLSI design platform. He is applying synchoros VLSI design to artificial neural networks, biologically plausible models of brain and complex multimedia and telecom applications.